Journal of
Nanoscience and Nanotechnology
Vol. 10, 3118–3122, 2010

Surface Plasmon Resonance Tuning of Silver Nanoparticle Array Produced by Nanosphere Lithography Through Ion Etching and Thermal Annealing

Kwang Hyun Baek, Jung Hoon Kim, Kil Bok Lee, Hyung Soo Ahnn, and Chong Seung Yoon*

Department of Materials Science and Engineering, Hanyang University, Seoul, 133-791, Republic of Korea

RESEARCH ARTICLE

It was demonstrated that size of the Ag nanoparticles array fabricated by nanosphere lithography (NSL) can be changed as needed by reactive ion etching (RIE) of the self-assembled polystyrene (PS) nanosphere template and post-annealing of the Ag particle array. A macroscopic 2D array of ordered Ag nanoparticles stretching over an area greater than 1 cm^2 was achieved using a modified nanosphere lithography method. The wavelength corresponding to the extinction maximum of the surface plasmon resonance (SPR) from the Ag nanoparticle array was systematically tuned by RIE of the PS template. Additional tuning of SPR was achieved by post-annealing the Ag nanoparticles which induced shape-changes in the Ag nanoparticles. We demonstrated that SPR can be tuned over the entire visible spectrum by RIE of the PS mask and thermal annealing, which can be potentially used to display localized SPR spectrum (hence, different color) throughout the visible range.

Keywords: Nanopattern, Polystyrene, Nanosphere Lithography, Surface Plasmon Resonance.

1. INTRODUCTION

Typical patterning process for fabricating a nanostructure array is based on photolithography[1] which is an integral part of the semiconductor technology. The conventional photolithographic method is, however, nearly approaching the resolution limit of less than 0.1 μm, dictated by physical laws. As an alternative for the photolithography, for a very high resolution patterning, electron beam lithography (EBL) can bring the resolution down to 5 nm.[2,3] However, because of the low throughput, it is difficult to create patterns over a large area (>1 mm^2) with EBL. In addition to the low throughput, EBL requires high capital investment. Such limitations make EBL unsuitable for general applications and confine its use to a laboratory practice. On the other hand, the nanosphere lithography (NSL) which uses a self-assembled template of polystyrene (PS) or silica beads offers a new opportunity to improve the controllability of the self-assembled system with little cost and provides a quick synthesis route so that NSL is a valuable tool for producing prototype nano-patterned samples.[4–6] Nanosphere monolayer masks have been prepared by various means, including electrophoresis,[7] electrostatic deposition,[8,9] spin-coating,[10–12] a controlled evaporation of a solvent from the solution containing latex particles[13–15] or non-photolithographic methods.[16] Most of the masks, however, contain structural defects such as grain boundaries, dislocations, and vacancies which disturbs the long-range ordering of the final structure.

Recently, a new technique for preparing defect-free long-range ordered nanosphere monolayer based on self-assembly at a liquid/gas interface was proposed.[17] In this paper, we modified the method to consistently produce a highly ordered 2-dimensional array of Ag nanoparticles which excites localized surface plasmon resonance (SPR). We demonstrate that the SPR generated by the Ag nanoparticles can be tuned by modifying the PS template through reactive ion etching. Localized SPR excited by such ordered noble-metal array exhibits selective photoabsorption, scattering, and local electromagnetic field enhancement.[18] These properties of SPR can lead new types of technologically important optical applications utilizing the SPR effect which allows concentration and controlled guide of light into structures that are much smaller than the wavelength of the propagating light.[19]

2. EXPERIMENTAL PROCEDURE

The long-rang ordered PS monolayer was prepared following the steps described by Rybczynski et al.[17] Procedure

*Author to whom correspondence should be addressed.

1533-4880/2010/10/3118/005 doi:10.1166/jnn.2010.2176

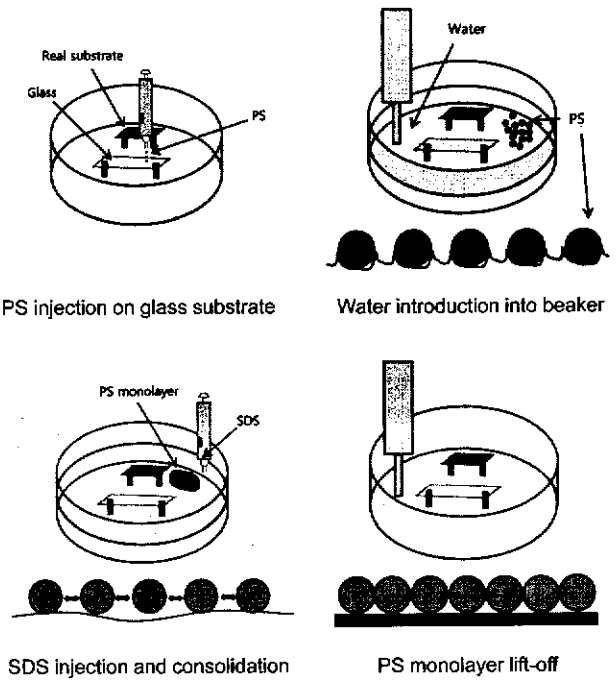

Fig. 1. Schematic diagram for preparing a hexagonal superlattice of PS beads.

for the preparation of the PS monolayer is schematically described in Figure 1. Monodisperse PS beads with a diameter of 460 nm (Bangs Laboratories, USA) was dispersed in water (10 wt%), which was further diluted with an equal amount of ethanol. 6 μl of the PS solution was then dropped onto the surface of a 2 cm × 6 cm glass substrate placed in a beaker. The beaker was cleaned with toluene to provide hydrophobic surface. Deionized water was then slowly injected into the beaker using a syringe. When the PS beads starts to float and form a loose monolayer on the water surface, 3~8 μl of 1% sodiumdodecylsulfate (SDS) solution was slowly introduced on the water surface. SDS caused the PS beads to consolidate into a tightly bound monolayer. The monolayer was then lifted from the water surface on a 1 cm × 1 cm glass substrate by extracting the water from the beaker. PS beads were thinned by reactive ion etching (RIE) in an argon–oxygen atmosphere. The chamber pressure was 58 mTorr and Ar and oxygen gas flow rates were 15 sccm and 30 sccm, respectively.

Ag nanoparticles were produced by depositing a thin layer of Ag onto the PS mask using a thermal evaporation system. Deposition rate was 1 nm/min, monitored by a quartz crystal thickness balance. After the deposition, the PS beads were removed from the sample in an ultrasonic bath of ethanol, leaving behind the patterned Ag nanoparticles. Samples subjected to post-deposition annealing were heat-treated at 300 °C for 1 h in vacuum condition (10^{-3} Pa). Atomic force microscopy (AFM, Parksystems XE-100), scanning electron microscopy (SEM, JSM 6330F) and transmission electron microscopy (TEM, JEOL 2010) were used to characterize the self-assembled polystyrene beads and nano-patterns. Optical absorption spectra were measured using a UV-VIS spectrometer (UV S-2100, SCHINCO).

3. RESULTS AND DISCUSSION

Figure 2 shows a typical SEM image of PS beads arranged into a closely packed monolayer produced using the self-assembling method at a liquid/gas interface described above. The image clearly manifests the long order obtained by self-assembly of the monodisperse PS beads. Fourier transform of the SEM image shown in the inset confirms that the PS beads were arranged into a perfect hexagonal superlattice. The superlattice extended over the entire substrate so that no domain boundaries were observed. Neither were there any visible large-scale defects such as dislocations although occasional point defects were observed. These point defects were mainly due to the effect of non-uniform nanosphere size. Cracks created during consolidation and lift-off process near the sample edge were also observed. Otherwise, we were able to consistently obtain a defect-free PS nanosphere superlattice based on the method described in Figure 1.

Because the PS beads can be cleanly dissolved from the substrate, such PS monolayer is ideally suited to serve as a shadow mask for metal deposition. Figure 3(a) presents a SEM image of a well-ordered array triangular-shaped (clearly visible in the inset) Ag nanoparticles produced by depositing 60-nm-thick Ag layer onto the PS nanosphere mask using a thermal evaporator and by removing the PS

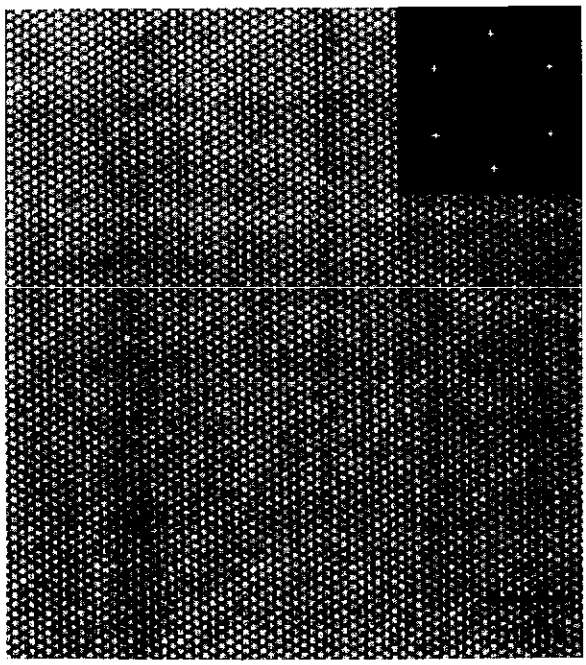

Fig. 2. SEM image of the ordered PS nanosphere monolayer with the inset showing Fourier transform of the image.

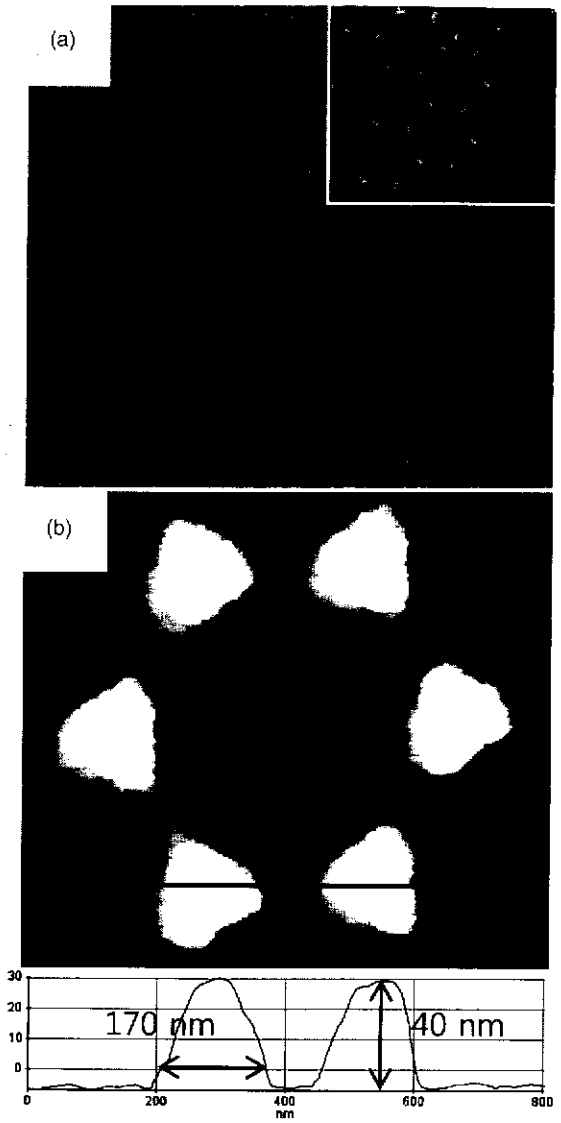

Fig. 3. (a) SEM image and (b) AFM image of ordered Ag nanoparticles produced by depositing 40-nm-thick Ag film onto the PS nanosphere monolayer and subsequently removing the PS beads. The profile below (b) shows the height and width of the Ag nanoparticles.

beads through ultrasonication in ethanol. The hexagonal superlattice was well transferred to the Ag nanoparticle array. The SEM image in Figure 3(a) also contains several interconnected groups of nanoparticles which were largely due to the size-distribution in the PS beads. Thus, the uniformity of the Ag nanoparticle size was mainly limited by polydispersity of the purchased PS beads. The Ag nanoparticles were, in fact, tetrahedral-shaped due to the shape of interstitial voids in the superlattice and the shadowing effect as verified by the AFM image in Figure 3(b). The Ag nanoparticles were 170 nm in width and 40 nm in height.

In order to be able to arbitrarily alter the final Ag nanoparticle size, diameter of the ordered PS beads were changed by RIE.[20] Figure 4(a) shows the PS masks etched

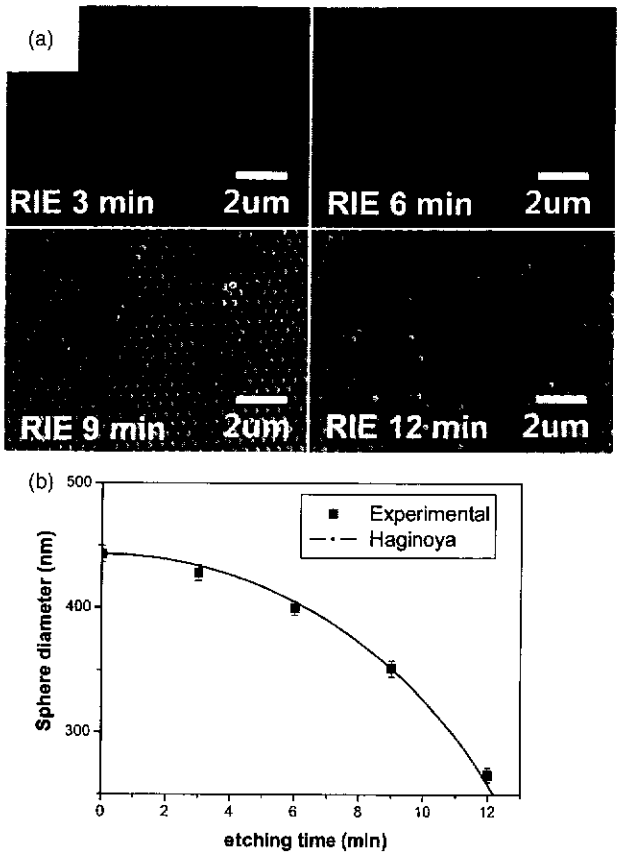

Fig. 4. (a) SEM images of the PS beads after RIE for different periods, (b) plot of the PS diameter versus etching time, fitted to the Haginoya's model with $k = 1$.

with RIE for various periods. The diameter of PS beads progressively decreased from 460 nm to 270 nm with increasing etching time while maintaining the hexagonal superlattice. However, when the etching period was extended to 12 min, the PS beads started to move out of registry. It appears that as the PS beads became increasingly smaller during 12 min of RIE, the kinetic energy imparted by the plasma was sufficiently large to overcome the binding energy and disturb the periodicity. Therefore, minimum diameter of the PS beads obtainable by RIE appears to be approximately 60% of the initial diameter. Meanwhile, the etched bead diameter well matched the Haginoya's empirical expression[20] which relates the etching time, t to the sphere diameter, d:

$$d = d_0 \cos\left[\sin^{-1}\left(\frac{kt}{2d_0}\right)\right] \quad (1)$$

where d_0 is the initial diameter of PS beads, and k is a constant depending on the etching conditions such as gas component, pressure, incident power, and temperature. Figure 4(b) clearly demonstrates the experimental data from the samples well-obeying the Haginoya's equation with $k = 1$. The decreased PS bead diameter enlarged the interstitial volume, hence, enabling control of the size of deposited Ag nanoparticles.

It is well known that the noble-metal nanoparticle arrays exhibit collective oscillations of conduction electrons known as surface plasmon when the nanoparticles are excited by light. The wavelength corresponding to the absorption maximum of the SPR is highly dependent on the size, shape, and surrounding dielectric properties of the metal nanoparticles.[18] Tuning of the extinction spectra over the entire visible spectrum was accomplished by controlling the size of Ag nanoparticles using RIE of the PS beads. Figures 5(a–c) a series of AFM images of the Ag nanoparticle arrays produced by the etched PS nanosphere masks. The width of the Ag nanoparticles increased as expected as the etching time increased whereas the height remained constant at 40 nm. After RIE of 1 min, the width of the Ag nanoparticles was 185 nm, which further increased to 205 nm when the RIE time was increased to 2 min. Corresponding normalized UV-visible extinction spectra from the samples in Figures 5(a–c), showing a single surface plasmon resonance peak, are shown Figure 5(d). As the Ag nanoparticles became increasingly large by RIE of the PS beads, the resonance peak also correspondingly red-shifted. The observed red shift in the resonance peak is consistent with previous results and is well-justified by classical Mie theory.[21] In addition to the main peak, each spectrum possessed a satellite peak at the blue end of the visible spectrum. SPR can be produced into two bands: longitudinal (in-plane) and transverse (normal to the substrate) directions of the nanoparticles. It is likely that the transverse mode created the resonance at about 410 nm while the longitudinal mode which strongly depends on the size of nanoparticles generated the main resonance peak. A strong electromagnetic coupling existing in the longitudinal direction due to the close end-to-end contact of the nanoparticles is responsible for the main resonance peak. In contrast, the transverse band was relatively weak and exhibited minimal dependence on the particle size because the nanoparticles were not coupled in the transverse direction.

Figure 6 plots the SPR peaks exhibited by the same set of samples in Figure 5 after annealing at 300 °C for 1 hour. Thermal annealing the Ag nanoparticle led to a marked blue shift of the resonance peak, causing dramatic changes in the color of the samples. The blue shift brought by thermal annealing was as large as 270 nm so that a SPR peak can potentially be generated from the red-end to the blue end, covering the entire visible spectrum as needed. The large blue shift is likely due to change in the shape of the Ag nanoparticles. An AFM image of the thermally annealed Ag nanoparticles in Figure 7(a) indicate that the particle shape changed from a tetrahedral shape to a near-spherical shape; i.e., the height of the particles increased while the width decreased substantially. Cross-sectional TEM images of the Ag particles before and after annealing at 300 °C in Figures 7(b and c) also verifies the particle shape change incurred during thermal annealing. Other contributing factors for the large blue shift were the decreased particle diameter and the subsequent increase in effective interparticle distance.[18] Figures 5 and 6 demonstrate that the SPR peak from the Ag nanoparticle array can be tuned as needed by altering the shape and size of the Ag nanoparticles through RIE of the PS mask and thermal annealing.

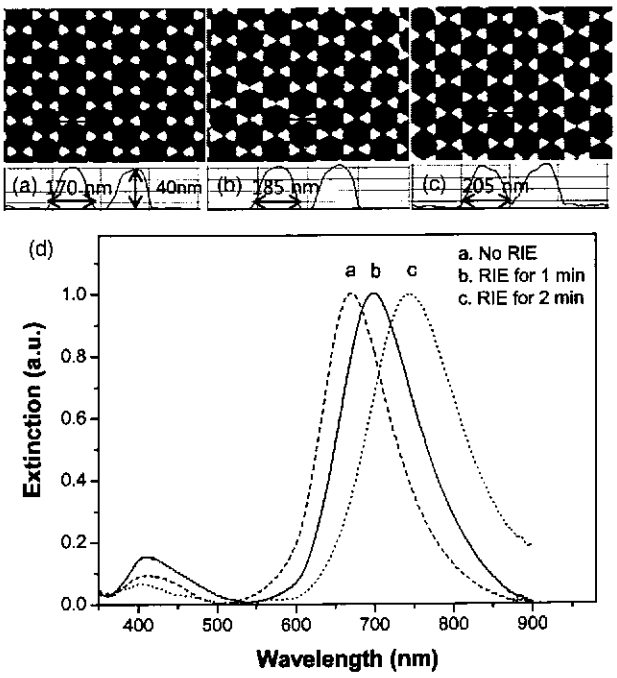

Fig. 5. AFM images (with corresponding profiles) of the Ag nanoparticle by depositing 60-nm-thick Ag film onto the PS masks etched for different periods: (a) no etching, (b) for 1 min, (c) for 2 min, (d) UV-visible extinction spectra from the samples (a)–(c).

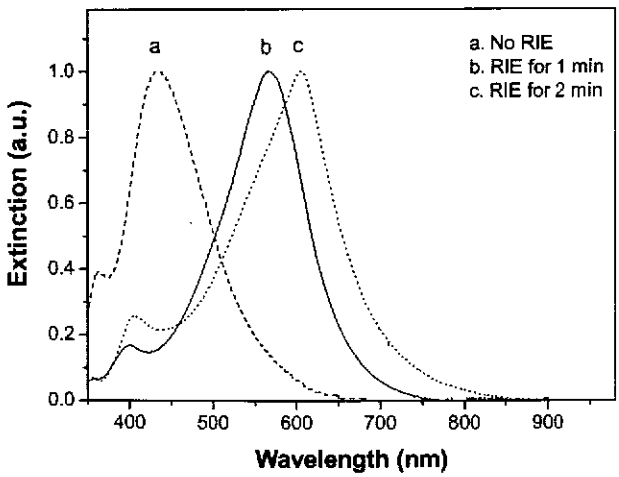

Fig. 6. UV-visible extinction spectra after annealing at 300 °C for 1 hour. The samples were prepared by depositing 60-nm-thick Ag film onto the PS masks etched for different periods.

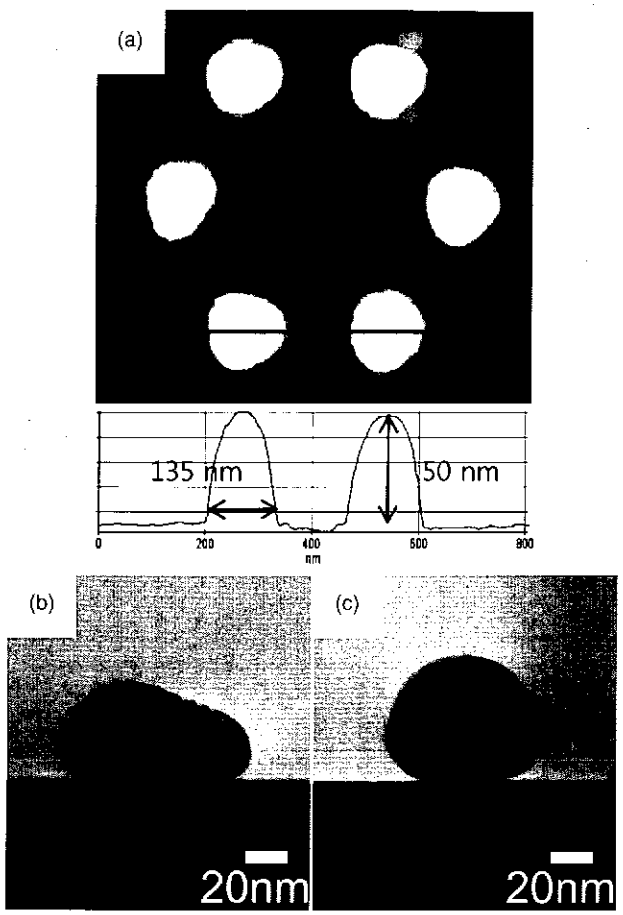

Fig. 7. (a) AFM image of the Ag nanoparticle array prepared by depositing 60-nm-thick Ag film onto the PS mask and annealed at 300 °C for 1 hour and cross-sectional TEM image of the Ag nanoparticle (b) before and (c) after annealing at 300 °C for 1 hour.

4. CONCLUSION

We demonstrated that SPR generated from a long-range ordered silver nanoparticles produced by NSL can be tuned by controlling both size and shape of the nanoparticles. Size of the Ag nanoparticles can be easily controlled by reducing the PS bead diameter through varying the etching time. SPR can be further tuned over the entire visible spectrum by simple thermal annealing without using PS beads of different sizes or changing the amount of metal deposited.

Acknowledgment: This work was supported by Hanyang Fusion Materials Program funded by Ministry of Education, Science and Technology, Korea and by the Korea Research Foundation Grant funded by the Korean Government (MOEHRD) (KRF-2006-005-J04103).

References and Notes

1. L. R. Hariott and R. Hull, Introduction to Nanoscale Science and Technology, 1st edn., edited by M. D. Ventra, S. Evoy, and J. R. Jr. Heflin, Kluwer acedimic Publishers, Norwell, Mass. (**2004**), p. 7.
2. B. Cui, W. Wu, L. S. Kong, X. Y. Sung, and S. Y. Chou, *J. Appl. Phys.* 85, 5534 (**1999**).
3. T. Ito and S. Okazaki, *Nature* 406, 1027 (**2000**).
4. S. M. Weekes, F. Y. Ogrin, and W. A. Murray, *Langmuir* 20, 11208 (**2004**).
5. G. Zhang and D. Wang, *J. Am. Chem. Soc.* 130, 5616 (**2008**).
6. A. Das, J. Zhao, G. C. Schatz, S. G. Sligar, and R. P. Van Duyne, *Anal. Chem.* 81, 3754 (**2009**).
7. M. Giersig and P. Mulvaney, *Langmuir* 9, 3408 (**1993**).
8. A. Rogach, A. Susha, F. Caruso, G. Sukhorukov, A. Kornowski, S. Kershaw, H. Möhwald, A. Eychmüller, and H. Weller, *Adv. Mater.* 12, 333 (**2000**).
9. H. W. Deckman and J. H. Dunsmuir, *Appl. Phys. Lett.* 41, 377 (**1982**).
10. J. C. Hulteen and R. P. Van Duyne, *J. Vac. Sci. Technol. A* 13, 1553 (**1995**).
11. J. C. Hulteen, D. A. Treichel, M. T. Smith, M. L. Duval, T. R. Jensen, and R. P. Van Duyne, *J. Phys. Chem.* 103, 3854 (**1999**).
12. M. Winzer, M. Kleiber, N. Dix, and R. Wiesendanger, *Appl. Phys. A* 63, 617 (**1996**).
13. R. Micheletto, H. Fukuda, and M. Ohtsu, *Langmuir* 11, 3333 (**1995**).
14. F. Burmeister, W. Badowsky, T. Braun, S. Wieprich, J. Boneberg, and P. Leiderer, *App. Surf. Sci.* 144–145, 461 (**1999**).
15. N. D. Denkov, O. D. Velev, P. A. Kralchevsky, I. B. Ivanov, H. Yoshimura, and K. Nagayama, *Langmuir* 8, 3183 (**1992**).
16. Y. Lu, Y. Yin, B. Gates, and Y. Xia, *Langmuir* 17, 6344 (**2001**).
17. J. Rybczynski, U. Ebels, and M. Giersig, *Colloids Surf. A* 219, 1 (**2003**).
18. T. R. Jensen, M. D. Malinsky, C. L. Haynes, and R. P. Van Duyne, *J. Phys. Chem. B* 104, 10549 (**2000**).
19. W. L. Barnes, A. Dereux, and T. W. Ebbeson, *Nature* 424, 824 (**2003**).
20. C. Haginoya, M. Ishibashi, and D. Koike, *Appl. Phys. Lett.* 71, 2934 (**1997**).
21. G. Mie, *Ann. Phys.* 25, 377 (**1908**).

Received: 25 May 2009. Accepted: 17 June 2009.